THE JOURNAL OF PHYSICAL CHEMISTRY C

Article

pubs.acs.org/JPCC

Temporally and Spatially Resolved Oxidation of Si(111)-(7 × 7) Using Kinetic Energy Controlled Supersonic Beams in Combination with Scanning Tunneling Microscopy

Bryan Wiggins, L. Gaby Avila-Bront,‡ Ross Edel, and S. J. Sibener*

The James Franck Institute and Department of Chemistry, The University of Chicago 929 East 57th Street, Chicago, Illinois 60637, United States

ABSTRACT: The site-specific locations of molecular oxygen reactivity on Si(111)-(7 × 7) surfaces were examined using kinetic energy selected supersonic molecular beams in conjunction with *in situ* scanning tunneling microscopy. We herein present a detailed visualization of the surface as it reacts in real-time and real-space when exposed to molecular oxygen with translational energy E_i = 0.37 eV. Atomically resolved images reveal two channels for oxidation leading to the formation of dark and bright reaction sites. The darks sites dominate the reaction throughout the range of exposures sampled and exhibit almost no preference for occurrence at the corner or inner adatom sites of the reconstructed (7 × 7) unit cell. The bright sites show a small preference for corner vs inner site reactivity on the reconstructed (7 × 7) unit cell. The bright site corner preference seen here at elevated kinetic energies and with selected incident kinematics is smaller than that typically observed for more conventional thermal (background dosed) oxidation processing. These observations suggest that two adsorption pathways, trapping-mediated chemisorption and direct chemisorption, occur simultaneously when using energetic molecular oxygen but with modified relative probability as compared with thermal dosing. These results demonstrate the efficacy of using angle- and energy-selected supersonic molecular beams to gain a topographical diagram of the accessible reactive potential surface energy and precise control of semiconductor oxidation, a process that is of growing importance as we seek to create high-quality and precisely defined oxides having atomic dimensions.

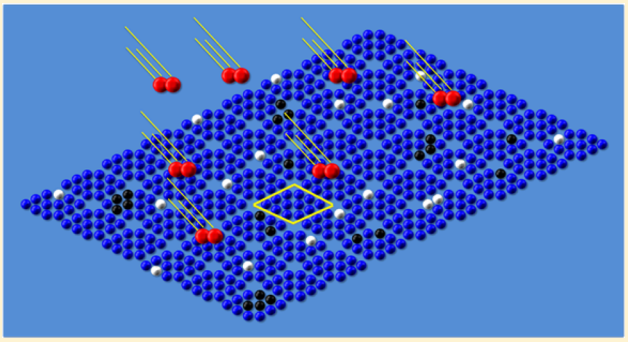

INTRODUCTION

The oxidation of silicon surfaces has received considerable attention over the past four decades, serving as a general model for semiconductor oxidation.[1−3] As devices continue to decrease in size and approach atomic dimensions, the challenge of producing thinner, homogeneous, and perfected oxide layers increases. Current metal oxide semiconductor field-effect transistors (MOS-FETs) utilize oxide layers approximately four atoms thick, and further improvements using existing methods have been evolving slowly. In order to gain more refined control over oxidation and to produce defect-free oxide monolayers, it is essential to understand the initial oxidation process at subnanometer dimensions with atomic resolution. FETs with 3D structures, such as fin-FETs, are one illustrative candidate for future devices; several studies have examined fin-FETs with gate oxides on Si(111) fin sidewalls.[4,5] It is therefore valuable to understand the mechanism of oxygen adsorption not only on Si(100), but also on other crystallographic planes as well. The complex Si(111)-(7 × 7) interface, due to the presence of several different inherent atomic sites within the reconstructed unit cell, presents a unique opportunity to examine complex oxidation processes on semiconductor surfaces.[6,7]

Numerous studies of oxygen adsorption on silicon have been conducted experimentally[8−11] and theoretically.[12−16] In particular, several groups have investigated silicon oxidation using scanning tunneling microscopy (STM).[17−20] These studies found that the adsorption of thermal O_2 on Si(111)-(7 × 7) produced bright and dark reaction sites at adatoms, with the oxide coverage increasing with oxygen exposure. It was determined that the bright sites are so-called *ins* × *n* (*n* = 1−3) structures with oxygen atoms inserted into the Si−Si backbond.[17,20,21] The ins × *n* configuration elevates the Si adatom relative to the surface plane, causing a bright contrast in the STM image.[17] The dark sites consist of so-called *ad-ins* × *n* structures with oxygen adsorbed directly on top of a previously reacted *ins* × *n* site; these are therefore products of a subsequent reaction that occurs under thermal conditions. The adsorption of oxygen on top of an adatom suppresses its dangling bond so that it appears as a dark contrast depression in STM images.[6] Furthermore, recent photoelectron studies suggest *ins* structures are the initial product of oxygen adsorption on Si(111)-(7 × 7).[22] First principle calculations

Received: February 9, 2016
Revised: March 24, 2016
Published: April 8, 2016

DOI: 10.1021/acs.jpcc.6b01360
J. Phys. Chem. C 2016, 120, 8191−8197

using a complete (7 × 7) unit cell have determined that chemisorbed molecular oxygen dissociates spontaneously upon adsorption without an activation barrier, creating *ins* × *n* primary products followed by *ad-ins* × *n* secondary products.[12] Throughout this article, we will interpret bright and dark sites as *ins* × *n* and *ad-ins* × *n* configurations, respectively. Figure 1 shows several possible *ins* and *ad* configurations.

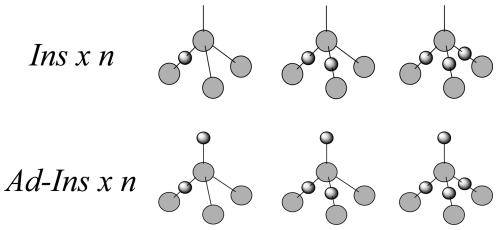

Figure 1. Ball and stick models of different oxygen adsorption configurations. Large circles represent Si atoms and small circles represent oxygen atoms; *n* is the number of oxygen inserted into the Si−Si bonds.

Supersonic molecular beams (SMBs) present an incisive tool for studying energetic site specific reactivity[23−26] on surfaces including oxygen.[27−30] Nolan and co-workers[31,32] report two types of molecular oxygen adsorption processes on Pt(111) depending on the incident translational energy (E_i). They utilized *in situ* high-resolution electron energy loss spectroscopy (HREELS) with SMBs to determine whether molecular oxygen experiences superoxo-like or peroxo-like precursor states prior to dissociating on the surface. High-kinetic-energy oxygen over the 0.2 to 1.37 eV range chemisorbs initially as a peroxo-like molecular species. On the other hand, at 0.055 eV they observed a high population of both superoxo-like and peroxo-like adsorbed oxygen. As with metal surfaces, the incident translational energy also plays a role in molecular oxygen adsorption on Si(111)-(7 × 7).[33−35] Yan et al.[33] performed an energy-dependent study with incident energies ranging from 0.02 to 0.25 eV. They observed no energy dependence for the formation of dark sites and found that bright site selectivity increases as a function E_i, with corner sites becoming more favorable at higher energies. They suggested two different molecular precursors resulting in the different oxygen−silicon configurations and attributed the kinetic energy dependence of bright site creation to the presence of multiple adsorption pathways: precursor-mediated chemisorption and direct activated chemisorption. Our current study builds on their early results with the additional capability of monitoring the exact scanning region over multiple oxygen exposures, i.e., with time resolution for visualization of the ongoing oxidation mechanism(s). Similarly, Yoshige and Teraoka[34,35] also report trapping-mediated chemisorption and direct chemisorption adsorption pathways for O_2 adsorption on Si(111)-(7 × 7). They monitored the change in photoelectron spectroscopy peaks while exposing the surface either to thermal (i.e., background dosed) or SMB molecular oxygen. The trapping state occurred for thermal O_2 adsorption, which has an average molecular kinetic energy defined by the most probable speed in the Maxwell−Boltzmann distribution of ∼0.03 eV, and also for SMB energies less than 0.06 eV. They suggest a mixture of mediated and direct chemisorption for energies ranging from 0.06 to 0.15 eV; however, at 0.39 eV only direct chemisorption was found.

The experimental findings with oxidation via supersonic oxygen beams clearly demonstrate that incident translational energy plays a role in the oxidation mechanism on the surface. SMBs are traditionally paired with nonlocal spectroscopy techniques (such as Auger, XPS, or HREELS) or configured in a way such that observing local chemical dynamics is not possible, thus obscuring the time-dependent atomic and nanoscale effects of energy and angle variation in the overall reaction mechanism. Therefore, we have constructed a new instrument that can provide time dependent and spatial resolution of interfacial reactivity as a function of translational kinetic energy with specified incident kinematic conditions.

In this study, we report a visual mapping of Si(111)-(7 × 7) oxidation at room temperature in real-space and real-time utilizing supersonic molecular beams with *in situ* scanning tunneling microscopy. High-resolution imaging reveals distinct adsorption chemistry for SMB O_2 in comparison with thermally dosed O_2. In addition, our studies provide insight into

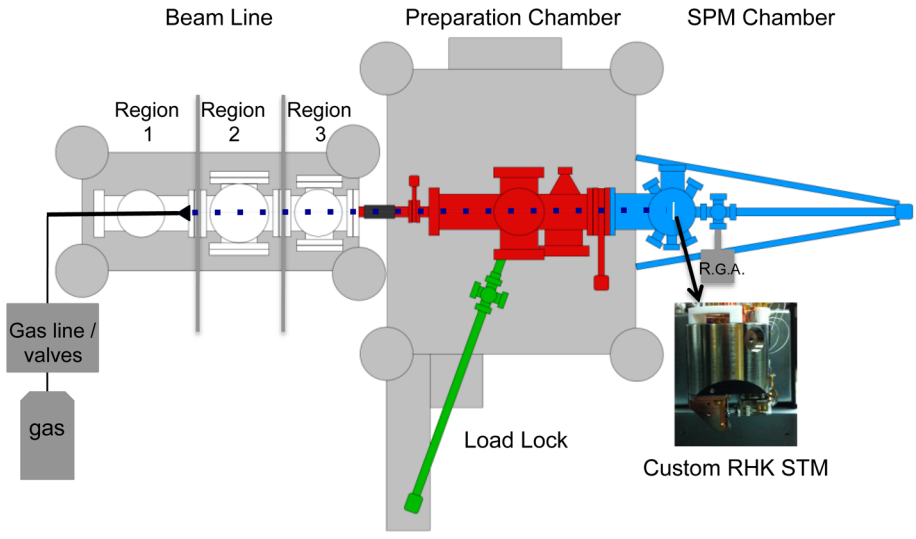

Figure 2. Top view schematic of the new supersonic molecular beam/SPM instrument with photo of the custom Pan-style STM/AFM: The sample's surface plane is vertical and oriented 45 degrees with respect to the incident beam direction.

DOI: 10.1021/acs.jpcc.6b01360
J. Phys. Chem. C 2016, 120, 8191−8197

atomically resolved site-specific oxidation at various locations within the unit cell for varied exposure levels over time. This combination of techniques allows us to study oxygen adsorption as a function of kinetic energy in an unprecedented fashion.

EXPERIMENTAL SECTION

Instrumentation: Gas-Surface Scattering Using Supersonic Molecular Beams (SMBs) Coupled with an Ultra-High Vacuum Scanning Tunneling Microscope (UHV-STM). A novel ultrahigh vacuum system equipped with a supersonic molecular beam and a custom scanning probe microscope with the surface plane normal to the beam (when the incident angle is set at 0° polar angle) is used in this study. This geometric arrangement allows us to perform real-time and real-space *in situ* imaging. The configuration is such that the STM assembly can independently rotate 0−50° for polar-angle-dependent studies. The tip has the capability to move in *XYZ* directions to precisely and repeatedly access different areas of the sample and remove the tip from the beam's line of sight for dosing in order to avoid shadowing. The SMB beamline consists of three differentially pumped stages separated by a skimmer (first stage) and a collimating aperture (second stage). The third and final stage houses the last collimating aperture, which determines the 4 mm beam spot size at the sample. Two Oerlikon Leybold 600 $L{\cdot}s^{-1}$ magnetically suspended turbomolecular pumps evacuate the first and second stages of the beamline. These pumps are backed by a single Edwards nXDS15i dry scroll pump. A 100 $L{\cdot}s^{-1}$ ion pump is used to evacuate the third region of the beamline. The first, second, and third differential region working pressures with the beam on are $\sim 10^{-4}$, 10^{-6}, and 10^{-9} Torr, respectively. The differentially pumped STM chamber, evacuated with ion and Ti sublimation pumps, has a base pressure better than 1×10^{-10} Torr and remains in the low 10^{-10} Torr region during beam exposure. As shown in Figure 2, the SMB is connected to the sample preparation chamber by custom metal bellows and a mini conflat gate valve. The SMB and STM systems rest on separate air leg isolation tables with the bellows providing additional vibration decoupling as well as lateral movement for beam alignment. The presence of the SMB chambers does not produce electrical or mechanical noise in the STM data; therefore, the beamline can remain in full operation between sample exposures.

Silicon (111)-(7 × 7) Preparation. N-type Si(111) substrates (0.001−0.006 Ω-cm) were used in this experiment. The samples were degassed at 700 °C overnight, followed by flashing to ∼1200 °C while maintaining a pressure of $\leq 7.5 \times 10^{-10}$ Torr. The surface temperature was monitored by a Mikiron infrared pyrometer and heated by applying current directly through the sample. Several areas on the surface were checked for cleanliness and (7 × 7) reconstruction by STM prior to oxygen exposure. Etched $Pt_{0.8}Ir_{0.2}$ tips were used for imaging.

Oxidation Methods. Supersonic beams of molecular oxygen (SMB−O_2) were generated by expanding a 5% O_2/95% He mixture through a 30 μm diameter molybdenum pinhole at 15 psi. A translational kinetic energy of 0.37 eV with an energy distribution width of $\Delta E/E$ = 0.28 was found using time-of-flight measurements. Equation 1 was used to calculate a flux of ca. 10^{11} molecules/cm^2/s. Here S is the pumping speed, ΔP is the change of pressure between beam on and off, and A_{spot} is the cross-sectional area of the beam at the sample. A residual gas analyzer was used to monitor the change in pressure in the STM chamber. An incident angle of 45° relative to the sample normal was used for all SMB exposures.

$$\Phi = \frac{S \times \Delta P}{KT \times A_{spot}} \quad (1)$$

RESULTS AND DISCUSSION

Figure 3 shows high resolution constant current STM images of the occupied and unoccupied states of Si(111)-(7 × 7). The

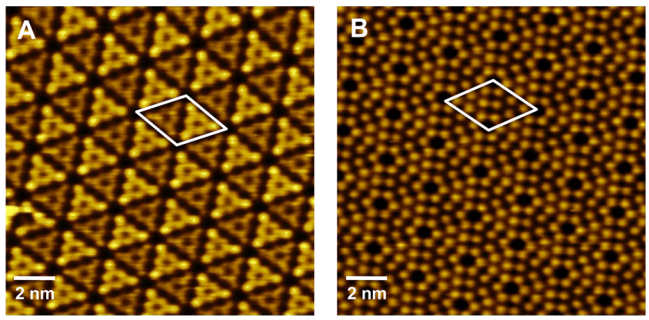

Figure 3. STM images showing (A) occupied (−1.3 V 200 pA) and (B) unoccupied states (2 V 200 pA) of a Si(111)-(7 × 7) surface. White overlay indicates the unit cell.

images adhere to Takayanagi's[36] dimer-adatom-stacking fault (DAS) model with the *faulted* (bright triangular region of the STM unit cell image) and *unfaulted* (dark triangular region of the STM unit cell image) subunits clearly visible when using negative scanning bias. The reconstructed unit cell contains 12 adatoms that provide direct bonding sites for oxygen molecules. The 12 adatoms can be divided into six corner and six inner adatoms; the corner adatoms are adjacent to corner holes that create a distinct local electronic environment compared to the inner adatoms. Our results agree with the trend of the initial oxidation reactivity showing preference for the faulted side of the unit cell.[37] The corner and inner preference will be discussed in greater detail below.

In order to obtain accurate statistical information on the surface at various stages of oxidation, oxidation sites were surveyed over scan areas roughly 50 × 50 nm in size. These images consisted of approximately 3500 to 4000 available adatoms, with typically less than 2% defect concentration prior to oxygen exposure. The tip was retracted during each exposure and subsequently brought back to the same location to examine the surface after reaction. The data were collected either as a series of sequential images of an identical area (reacquired using surface defects or prior oxidation sites for absolute positioning) or statistically using nearby regions located micrometers apart. The surface reactivity shows good reproducibility within the expected statistics over multiple exposures. Figure 4 shows three images in the same scan area, after three different SMB−O_2 exposures. High-resolution STM images revealed both dark (D) and bright (B) sites dispersed heterogeneously across the surface after exposure to SMB−O_2.

Previous studies of thermal oxidation via background gas dosing show bright and dark sites have approximately a 1:1 concentration ratio at low exposures (<0.6 L); only after additional oxidation do the dark sites start to dominate.[15] The surface becomes disordered and the (7 × 7) reconstruction is lifted at high oxygen exposures.[1,37] In contrast to the

DOI: 10.1021/acs.jpcc.6b01360
J. Phys. Chem. C 2016, 120, 8191−8197

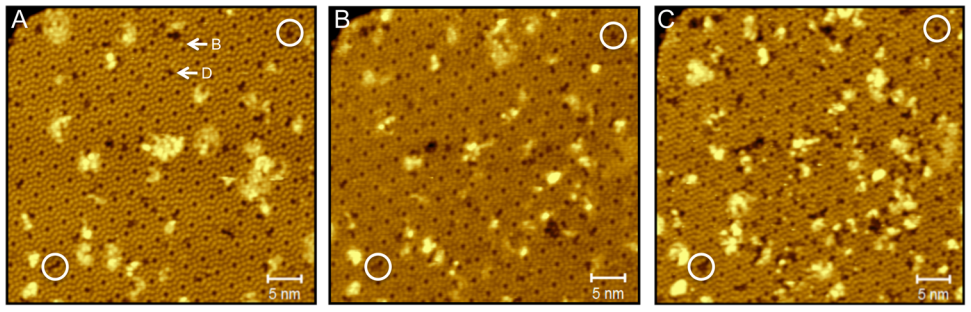

Figure 4. STM images in the same scan area after multiple SMB−O_2 exposures. Circles are used as reference points. The images display bright (*ins*) and dark (*ad*) features distributed heterogeneously across the surface. The *ad* structures dominate the adsorption type even at low surface coverage. All images were recorded at 2 V and 200 pA.

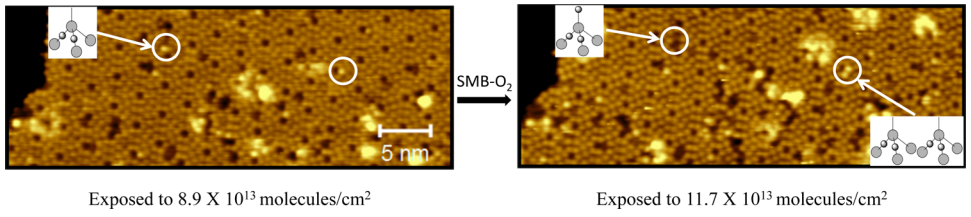

Figure 5. STM images of atomic level oxidation at two sequential exposure times, t = 3 min and t = 4 min. Circles indicate areas of change, e.g., a bright site converting to dark after additional SMB−O_2 exposure, and an area where a single bright site changed into a pair of adjacent bright sites. Images were taken at 2 V and 230 pA.

background gas dosing outcome, we found a predominance of dark sites throughout the SMB−O_2 oxidation process including at initial low exposures. However, the bright sites show some resemblance to outcomes observed using background gas dosing. Recently, Onoda et al.[38] addressed the question of what happens to the atomic oxygen after the molecular species dissociate on Si(111)-(7 × 7) at room temperature by utilizing scanning probe microscopy and density functional theory calculations. Their AFM images show bright sites that were either in pairs on adjacent Si adatoms or isolated single sites without another bright site in the immediate surroundings. They identified the bright sites in pairs as two adjacent *ins* × 1 structures, with one O atom inserted in a Si adatom's backbond, whereas single bright sites were ascribed to *ins* × 2 configurations, with two O atoms inserted into the backbonds of one Si adatom (see Figure 1). The experiments also illustrated the conversion of bright sites to dark sites after additional oxidation with the addition of an O atom on the top site of a previously reacted adatom. Our SMB results are in agreement with the dominance of single over paired bright sites found in their thermally dosed experiment. However, Figure 5 displays sequential images in the same location that exhibit a single bright site becoming paired after further oxidation, implying that some of the pairs may actually be two *ins* ×2 sites adjacent to one another. Figure 5 also highlights a bright site converting into a dark site after additional oxygen exposure. This follows the conventional oxidation scheme of an *ins* × *n* site undergoing a secondary oxidation reaction and becoming an *ad-ins* × *n* site. These results show that the initial oxidation process can be complex and reveal new insight that was not previously available without the ability to obtain atomic resolution of the same location over multiple SMB−O_2 exposures.

Atomic resolution images allow us to discern spatial, site-specific information for the reacted Si adatoms. A (7 × 7) lattice was used to manually determine the number of adatoms and/or reacted sites present in each image. Only areas that show clear Si adatoms or reacted sites were used in the calculations to create the data shown in Figures 6 and 8. Previous defects prior to oxygen exposure and tip artifacts (bright clouds) were discarded in the total number of available sites. The graph in Figure 6a shows that the overall reactivity follows a linear trend, while the data in Figure 6b reveal that this linear behavior is a result of the relative reaction probabilities for dark and bright outcomes under the chosen reaction conditions, nonlinear behavior might occur for different reaction conditions that influence the relative probabilities of bright vs dark site creation. An initial sticking probability of ∼0.1 was determined using the calculated flux of the impinging molecules, the change in defect coverage, and the surface density of available adatoms.

Bright and Dark Site Reactivity. Figure 6b shows the coverage of bright or dark sites relative to the overall number of available sites. As mentioned above, previous thermal oxidation experiments report a roughly equal number of bright and dark sites on the surface for the early stages of oxidation. Interestingly, at similar exposures by SMB−O_2, dark sites dominate the adsorption process. This is a notable finding as the oxygen−silicon configuration during the early oxidation stages is altered by the use of SMB exposure. Congruent with the overall reactivity, the dark site coverage increases linearly as a function of oxygen exposure. On the other hand, the bright site coverage remains ∼4% throughout multiple exposures, which is a lower steady state point than the 10% previously found by thermal studies.[39] Figure 7 shows a large scan area of the surface with ∼14% of the available adatoms reacted after SMB−O_2 exposure. The dark sites have increased significantly in number and started to form islands (i.e., groups or clusters of reacted sites), whereas bright sites are still dispersed across the surface and occupy a low percentage of the surface. On the

DOI: 10.1021/acs.jpcc.6b01360
J. Phys. Chem. C 2016, 120, 8191−8197

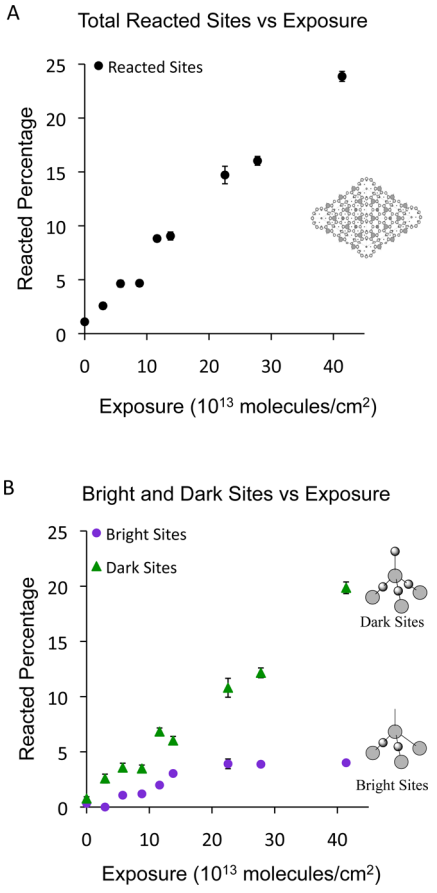

Figure 6. (A) Reactivity vs time for the entire surface. (B) Decomposition of the overall reactivity into the percentage of *dark* and *bright* structures found on the surface vs time. Note that bright and dark sites correspond to various *ins* × *n* and *ad-ins* × *n* structures, respectively, where *n* = 1, 2, or 3. Each point represents an STM image that contained approximately 4000 possible reaction sites. Some of the points represent statistics garnered from combining the results from multiple images. Error bars were generated by sample size counting statistics.

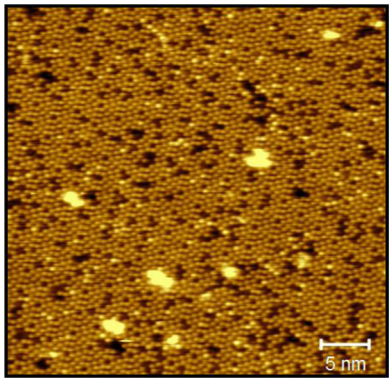

Figure 7. Large scale image after 2.8×10^{14} molecules/cm^2 SMB−O_2 exposure. The dark sites are beginning to form regions of adjacently reacted sites, referred to as clusters or islands of reacted areas, whereas the majority of bright sites remain isolated and are therefore not in contact with another bright site. Set point: 1.8 V, 250 pA.

basis of sequential images showing the creation and subsequent conversion of bright sites, we estimate the probability for the primary reaction of an unreacted adatom with a given O_2 molecule is ∼0.05, which is similar to that for thermal oxidation.[39,40] On the other hand, the secondary reaction probability of a bright site is higher (up to twice as reactive) when exposed to energetic and 45 deg incident polar angle SMB−O_2 as opposed to the probability found for thermal background dosed oxygen.[39,40] The increased probability of secondary reaction for bright sites converting to dark sites accounts for the low concentration of bright sites and cluster formation of dark sites after multiple oxidation exposures as discussed previously in Figure 6.

Corner and Inner Site Reactivity. We have also examined the site selectivity of bright and dark structures for corner and inner adatoms. In general, very little difference is seen. Upon close examination of bright site formation, we find a small preference for corner reactivity vs inner sites. The dark sites show very little preference, with perhaps a slight bias toward inner site reactivity, as shown in Figure 8. We note that

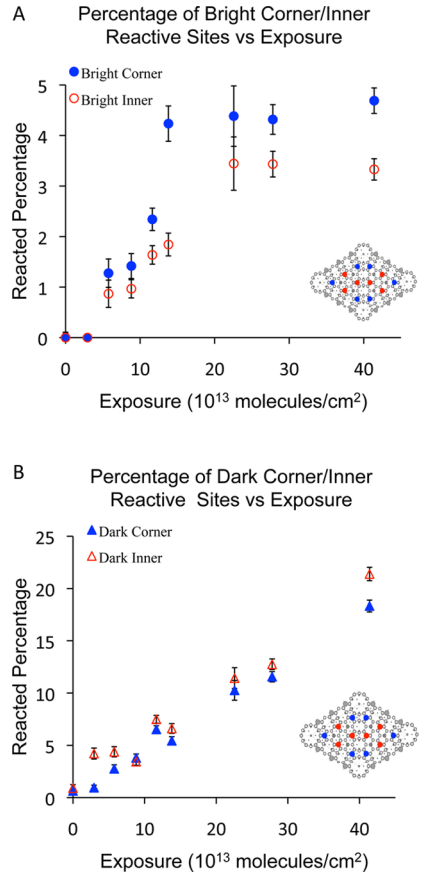

Figure 8. (A) Reactivity at corner and inner adatom sites for bright site formation. (B) Reactivity at corner and inner adatom sites for dark site formation. Corner and inner adatom symbols are filled and unfilled, respectively. The uncertainties are standard errors determined by sample size counting statistics. Inset: A schematic of the Si(111)-(7 × 7) dimer-adatom-stacking fault model with corner (blue) and inner (red) adatoms highlighted.

oxidation using energetic molecular oxygen does indeed differ from thermal processing with background gas dosing, with the bright sites created via SMB exhibiting a lower preference of ∼1.2:1 for corner sites, as compared to 2.0−4.0 as previously cited for thermal O_2.[18,41,42] The dark sites overall exhibit a ∼1:1 site selectivity, and in fact dark sites without an observed bright intermediate prefer inner adatoms. This indicates that dark sites are also produced by a process other than the

DOI: 10.1021/acs.jpcc.6b01360
J. Phys. Chem. C 2016, 120, 8191−8197

conversion of bright sites, leading to different site selectivity. Thus, the conversion of bright sites upon further local reaction together with the direct formation of dark sites leads to the formation of islands (clustered regions) of dark sites. For thermal O_2, where trapping-mediated chemisorption dominates the adsorption process, the initial oxidation readily occurs at the corner sites, likely due to the corner adatoms' strain energy associated with their unique environment within the (7 × 7) unit cell.[18] The observed lower selectivity when using translationally fast O_2 is consistent with a higher overall probability for direct chemisorption occurring across the unit cell,[34] that is, more regions of the operative potential energy surface become accessible to O_2 reactivity due to the higher energy of the incident molecular ensemble. According to the potential energy surface diagram for the O_2 adsorption on Si(111)-(7 × 7) found in ref 35, there are barriers of 0.06 and 0.39 eV. At energies ≤0.06 eV the molecules can enter a trapping state and diffuse across the surface to the preferred dissociate site (corner site). At our elevated translational energy of 0.37 eV, the molecules have enough energy to overcome the first barrier and reach the next region where O_2 more readily dissociates at its adsorption location with equal probabilities for occurring at a corner or inner site.

CONCLUSION

The site-specific locations of molecular oxygen reactivity on Si(111)-(7 × 7) surfaces were examined using kinetic-energy-selected supersonic molecular beams of molecular oxygen in conjunction with *in situ* scanning tunneling microscopy. We presented a detailed visualization of the surface as it reacts in real-time and real-space when exposed to molecular oxygen with translational energy E_i = 0.37 eV. Atomically resolved STM images reveal two channels for oxidation leading to the formation of dark and bright reaction sites. Sequential images show the overall reactivity increases linearly with respect to oxygen exposure. In contrast to thermal oxidation, the dark sites dominate the reaction throughout the range of exposures sampled, but exhibit no statistical preference for corner or inner adatom sites of the reconstructed (7 × 7) unit cell. The bright sites show a small preference for corner vs inner site reactivity on the reconstructed (7 × 7) unit cell. The bright site corner preference seen here at elevated kinetic energies and with selected incident kinematics is smaller than that typically observed for more conventional thermal (background dosed) oxidation processing. Under the reaction conditions used in this study, the bright sites have a population that reaches a steady state at about 4% of surface coverage. The increased probability of secondary reaction for bright sites converting to dark sites accounts for the low concentration of bright sites and cluster formation of dark sites after multiple oxidation exposures. These observations suggest that two adsorption pathways, trapping-mediated chemisorption and direct chemisorption, occur simultaneously when using energetic molecular oxygen but with modified relative probability as compared with thermal dosing. These results demonstrate the efficacy of using angle- and energy-selected supersonic molecular beams to gain a topographical diagram of the accessible reactive potential surface energy and precise control of semiconductor oxidation. Such precise control over interface oxidation is important, and will contribute to the development of more efficacious processing for the creation of high-quality and precisely defined oxides that are on the order of atomic dimensions.

AUTHOR INFORMATION

Corresponding Author

*(S.J.S.) E-mail: s-sibener@uchicago.edu. Telephone: 773-702-7193.

Present Address

‡Department of Chemistry, College of the Holy Cross, Worcester, MA

Notes

The authors declare no competing financial interest.

ACKNOWLEDGMENTS

This work was supported by the Air Force Office of Scientific Research, Grant Nos. FA9550-10-1-0219 and FA9550-15-1-0428, the AFOSR-DURIP program via Grant No. AFOSR-FA9550-09-1-0411, with early funding from the National Science Foundation via Grant No. NSF-CHE-0911424. Infrastructure support from the NSF-Materials Research Science and Engineering Center at the University of Chicago, Grant No. NSF-DMR-14-20709, is also gratefully acknowledged.

REFERENCES

(1) Engel, T. The Interaction of Molecular and Atomic Oxygen with Si (100) and Si (111). *Surf. Sci. Rep.* **1993**, *18*, 93−144.

(2) Chabal, Y. J. *Fundamental Aspects of Silicon Oxidation*; Springer-Verlag: Berlin and Heidelberg, Germany, 2001.

(3) Stiévenard, D.; Legrand, B. Silicon Surface Nano-Oxidation Using Scanning Probe Microscopy. *Prog. Surf. Sci.* **2006**, *81*, 112−140.

(4) Okuyama, K.; Sugimura, A.; Sunami, H. Optimized Silicidation Technique for Source and Drain of Fin-Type Field-Effect Transistor. *Jpn. J. Appl. Phys.* **2008**, *47*, 2407−2409.

(5) Liu, Y.; Sugimata, E.; Ishii, K.; Masahara, M.; Endo, K.; Matsukawa, T.; Yamauchi, H.; O'uchi, S.; Suzuki, E. Experimental Study of Effective Carrier Mobility of Multi-Fin-Type Double-Gate Metal−Oxide−Semiconductor Field-Effect Transistors with (111) Channel Surface Fabricated by Orientation-Dependent Wet Etching. *Jpn. J. Appl. Phys.* **2006**, *45*, 3084−3087.

(6) Martel, R.; Avouris, P.; Lyo, I. W. Molecularly Adsorbed Oxygen Species on Si (111)-(7 × 7): STM-Induced Dissociative Attachment Studies. *Science* **1996**, *272*, 385−388.

(7) Jensen, J. A.; Yan, C.; Kummel, A. C. Direct Chemisorption Site Selectivity for Molecular Halogens on the Si(111)- (7 × 7) Surface. *Phys. Rev. Lett.* **1996**, *76*, 1388−1391.

(8) Kim, K.-Y.; Shin, T.-H.; Han, S.-J.; Kang, H. Identification of the Precursor State in the Initial Stages of Si (111)-(7 × 7) Oxidation. *Phys. Rev. Lett.* **1999**, *82*, 1329−1332.

(9) Höfer, U.; Morgen, P.; Wurth, W.; Umbach, E. Initial Stages of Oxygen Adsorption on Si(111). II. The Molecular Precursor. *Phys. Rev. B: Condens. Matter Mater. Phys.* **1989**, *40*, 1130−1145.

(10) Gupta, P.; Mak, C. H.; Coon, P. A.; George, S. M. Oxidation Kinetics of Si (111)-7 × 7 in the Submonolayer Regime. *Phys. Rev. B: Condens. Matter Mater. Phys.* **1989**, *40*, 7739−7749.

(11) Okuyama, H.; Aruga, T.; Nishijima, M. Vibrational Characterization of the Oxidation Products on Si(111)-(7 × 7). *Phys. Rev. Lett.* **2003**, *91*, 256102.

(12) Niu, C.-Y.; Wang, J.-T. Adsorption and Dissociation of Oxygen Molecules on Si (111)-(7 × 7) Surface. *J. Chem. Phys.* **2013**, *139*, 194709.

(13) Lee, S.-H.; Kang, M.-H. Electronic and Vibrational Properties of Initial-Stage Oxidation Products on Si (111)-7 × 7. *Phys. Rev. B: Condens. Matter Mater. Phys.* **2000**, *61*, 8250−8255.

(14) Lee, S.-H.; Kang, M.-H. Identification of the Initial-Stage Oxidation Products on Si(111)-7 × 7. *Phys. Rev. Lett.* **1999**, *82*, 968−971.

(15) Schubert, B.; Avouris, P.; Hoffmann, R. A Theoretical Study of the Initial Stages of Si (111)−7 × 7 Oxidation. I. The Molecular Precursor. *J. Chem. Phys.* **1993**, *98*, 7593−7605.

DOI: 10.1021/acs.jpcc.6b01360
J. Phys. Chem. C 2016, 120, 8191−8197

(16) Schubert, B.; Avouris, P.; Hoffmann, R. A Theoretical Study of the Initial Stages of Si (111)−7 × 7 Oxidation. II. The Dissociated State and Formation of SiO_4. *J. Chem. Phys.* **1993**, *98*, 7606−7612.
(17) Avouris, P.; Lyo, I.-W.; Bozso, F. Atom-Resolved Surface Chemistry: The Early Steps of Si (111)-7 × 7 Oxidation. *J. Vac. Sci. Technol., B: Microelectron. Process. Phenom.* **1991**, *9*, 424−430.
(18) Lyo, I. W.; Avouris, P.; Schubert, B.; Hoffmann, R. Elucidation of the Initial Stages of the Oxidation of Silicon (111) Using Scanning Tunneling Microscopy and Spectroscopy. *J. Phys. Chem.* **1990**, *94*, 4400−4403.
(19) Leibsle, F. M.; Samsavar, A.; Chiang, T.-C. Oxidation of Si (111)-7 × 7 as Studied by Scanning Tunneling Microscopy. *Phys. Rev. B: Condens. Matter Mater. Phys.* **1988**, *38*, 5780−5784.
(20) Mayne, A. J.; Rose, F.; Comtet, G.; Hellner, L.; Dujardin, G. Variable Temperature STM Studies of the Adsorption of Oxygen on the Si(1 1 1)-7 × 7 Surface. *Surf. Sci.* **2003**, *528*, 132−137.
(21) Kinahan, N. T.; Meehan, D. E.; Narushima, T.; Sachert, S.; Boland, J. J.; Miki, K. Site-Specific Evolution of Surface Stress during the Room-Temperature Oxidation of the Si (111)-(7 × 7) Surface. *Phys. Rev. Lett.* **2010**, *104*, 146101.
(22) Yoshigoe, A.; Teraoka, Y. Immediate Product after Exposing Si (111)-7 × 7 Surface to O_2 at 300 K. *Jpn. J. Appl. Phys.* **2010**, *49*, 115704.
(23) Lee, D. Y.; Kautz, N. A.; Kandel, S. A. Reactivity of Gas-Phase Radicals with Organic Surfaces. *J. Phys. Chem. Lett.* **2013**, *4*, 4103−4112.
(24) Lee, D. Y.; Kandel, S. A. Communication: Site-Dependent Reactivity between Chlorine Atoms and Mixed-Chain-Length Alkanethiolate Monolayers. *J. Chem. Phys.* **2013**, *139*, 161103.
(25) Hundt, P. M.; Jiang, B.; van Reijzen, M. E.; Guo, H.; Beck, R. D. Vibrationally Promoted Dissociation of Water on Ni(111). *Science* **2014**, *344*, 504−507.
(26) Campbell, V. L.; Chen, N.; Guo, H.; Jackson, B.; Utz, A. L. Substrate Vibrations as Promoters of Chemical Reactivity on Metal Surfaces. *J. Phys. Chem. A* **2015**, *119*, 12434−12441.
(27) Moritani, K.; Okada, M.; Teraoka, Y.; Yoshigoe, A.; Kasai, T. Kinetics of Oxygen Adsorption and Initial Oxidation on Cu (110) by Hyperthermal Oxygen Molecular Beams. *J. Phys. Chem. A* **2009**, *113*, 15217−15222.
(28) Rettner, C. T.; Mullins, C. B. Dynamics of the Chemisorption of O_2 on Pt (111): Dissociation via Direct Population of a Molecularly Chemisorbed Precursor at High Incidence Kinetic Energy. *J. Chem. Phys.* **1991**, *94*, 1626−1635.
(29) Davis, J. E.; Nolan, P. D.; Karseboom, S. G.; Mullins, C. B. Kinetics and Dynamics of the Dissociative Chemisorption of Oxygen on Ir(111). *J. Chem. Phys.* **1997**, *107*, 943−952.
(30) Sjövall, P.; Uvdal, P. Oxygen Sticking on Pd(111): Double Precursors, Corrugation and Substrate Temperature Effects. *Chem. Phys. Lett.* **1998**, *282*, 355−360.
(31) Nolan, P. D.; Lutz, B. R.; Tanaka, P. L.; Davis, J. E.; Mullins, C. B. Molecularly Chemisorbed Intermediates to Oxygen Adsorption on Pt (111): A Molecular Beam and Electron Energy-Loss Spectroscopy Study. *J. Chem. Phys.* **1999**, *111*, 3696−3704.
(32) Nolan, P. D.; Lutz, B. R.; Tanaka, P. L.; Davis, J. E.; Mullins, C. B. Translational Energy Selection of Molecular Precursors to Oxygen Adsorption on Pt (111). *Phys. Rev. Lett.* **1998**, *81*, 3179−3182.
(33) Yan, C.; Jensen, J. A.; Kummel, A. C. Scanning Tunneling Microscopy of the Effect of Incident Energy upon Chemisorption Sites for O_2/Si(111)-7 × 7. *J. Chem. Phys.* **1996**, *105*, 773−778.
(34) Yoshigoe, A.; Teraoka, Y. Synchrotron Radiation Photoelectron Spectroscopy Study on Oxide Evolution during Oxidation of a Si(111)-7 × 7 Surface at 300 K: Comparison of Thermal Equilibrium Gas and Supersonic Molecular Beams for Oxygen Adsorption. *J. Phys. Chem. C* **2014**, *118*, 9436−9442.
(35) Yoshigoe, A.; Teraoka, Y. Adsorption Dynamics on Si (111)-7 × 7 Surface Induced by Supersonic O_2 Beam Studied Using Real-Time Photoelectron Spectroscopy. *J. Phys. Chem. C* **2010**, *114*, 22539−22545.
(36) Takayanagi, K.; Tanishiro, Y.; Takahashi, M.; Takahashi, S. Structural Analysis of Si (111)-7 × 7 by UHV-Transmission Electron Diffraction and Microscopy. *J. Vac. Sci. Technol., A* **1985**, *3*, 1502−1506.
(37) Yoshigoe, A.; Teraoka, Y. Atomic Lineation of Products during Oxidation of Si (111)-7 × 7 Surface Using O_2 at 300 K. *J. Phys. Chem. C* **2012**, *116*, 4039−4043.
(38) Onoda, J.; Ondráček, M.; Yurtsever, A.; Jelínek, P.; Sugimoto, Y. Initial and Secondary Oxidation Products on the Si (111)-(7 × 7) Surface Identified by Atomic Force Microscopy and First Principles Calculations. *Appl. Phys. Lett.* **2014**, *104*, 133107.
(39) Dujardin, G.; Mayne, A.; Comtet, G.; Hellner, L.; Jamet, M.; Le Goff, E.; Millet, P. New Model of the Initial Stages of Si(111)-(7 × 7) Oxidation. *Phys. Rev. Lett.* **1996**, *76*, 3782−3785.
(40) Pelz, J. P.; Koch, R. H. Successive Oxidation Stages and Annealing Behavior of the Si (111) 7 × 7 Surface Observed with Scanning Tunneling Microscopy and Scanning Tunneling Spectroscopy. *J. Vac. Sci. Technol., B: Microelectron. Process. Phenom.* **1991**, *9*, 775−778.
(41) Hasegawa, T.; Kohno, M.; Hosoki, S. Initial Stage of Oxygen Adsorption onto a Si (111)−7 × 7 Surface Studied by Scanning Tunneling Microscopy. *Jpn. J. Appl. Phys.* **1994**, *33*, 3702−3705.
(42) Pelz, J. P.; Koch, R. H. Successive Oxidation Stages of Adatoms on the Si (111) 7 × 7 Surface Observed with Scanning Tunneling Microscopy and Spectroscopy. *Phys. Rev. B: Condens. Matter Mater. Phys.* **1990**, *42*, 3761−3765.

DOI: 10.1021/acs.jpcc.6b01360
J. Phys. Chem. C 2016, 120, 8191−8197